metals

MDPI

Article

Modification of Porous Aluminum by Cold Rolling for Low-Noise Trailing Edge Applications

Jörn Tychsen *, Nicolas Lippitz and Joachim Rösler

Institute for Materials, TU Braunschweig, Langer Kamp 8, D-38106 Braunschweig, Germany; n.lippitz@tu-braunschweig.de (N.L.); j.roesler@tu-braunschweig.de (J.R.)

* Correspondence: j.tychsen@tu-braunschweig.de; Tel.: +49-531-391-3067; Fax: +49-531-391-3058

Received: 13 July 2018; Accepted: 26 July 2018; Published: 31 July 2018

Abstract: Noise reduction of aircrafts during take-off and landing has become an important part of research in aviation. The circulation of air around the airframe is a major source of noise during landing. This includes noise generated at the trailing edge. Open porous materials, such as porous aluminum, are investigated for the reduction of this noise. In this study, cold rolling is used to enhance the structure of porous aluminum in matters of aeroacoustics and mechanical properties. An important parameter characterizing the acoustic behavior is flow resistivity which is measured using the alternating airflow method. The flow resistivity is highly dependent upon the pore structure which is analyzed using three-dimensional computer tomography (CT). Additionally, CT combined with discontinuous tensile testing is used to study the influence of cold rolling on the damage behavior of porous aluminum. Besides the damage behavior, mechanical parameters have been determined to identify reasonable degrees of deformation. A cold rolling technique to produce material with a gradient in porosity is described and experimental porous trailing edges for measurements in an acoustic wind tunnel are shown. The findings of this study show that cold rolling is a promising way to customize porous aluminum for low-noise trailing edge applications.

Keywords: porous aluminum; graded; flow resistivity; cold rolling; damage behavior; CT; noise

1. Introduction

The growth of cities has led to site development for residential buildings in areas close to airports where aircraft noise is a major issue for residents [1–3]. Furthermore, there has been an increase in flight numbers for passenger transportation as well as commercial transport. For this reason, the reduction of aircraft noise became an important part of research in aviation. Due to the atmospheric absorption of noise between aircraft and ground at flight altitude the reduction of noise by engineering solutions is especially important during take-off and landing where aircrafts are close to the ground. Being in approach for landing, a major part of noise is generated by the circulation of air along the airframe. The trailing edge of the wing is one of the main acoustic sources at the airframe, which can be diminished by using open porous materials in the trailing edge [4–6]. Herr et al. [6] used different porous materials in an acoustic wind tunnel experiment, to analyze the effects of porous materials as trailing edges. The reduction of the sound pressure level for a broad frequency range is shown. One of the materials used as low-noise trailing edge is porous aluminum (PA) from "Exxentis" (Wettingen, Switzerland). The results reveal that additional noise is generated due to the sudden change from solid to porous material and the edges of pores orientated crosswise to the direction of flow. A promising technique to control these effects is cold rolling. It provides the possibility to produce a porosity gradient and may lead to elongated pores in the rolling direction.

In preliminary studies [7–10], different aspects of the deformation behavior of porous materials have been shown. Porous aluminum made out of AlSi7Mg is characterized as received in [10]. In [7]

different degrees of deformation were used to deform porous aluminum. The general possibility of changing the porosity, pore shape and pore size with a cold rolling process is shown. Based on those results, the possibility of adapting specific flow resistivity in a broad range is shown in [8] whereas the influence of cold rolling on the yield strength is shown in [9]. Further analysis of mechanical behavior (the damage behavior in particular), has neither been characterized for porous aluminum as received nor for cold-rolled material. Besides, it remains unclear how the findings can be used to address the shortcomings of porous materials for low-noise trailing edge applications noticed by Herr et al. [6].

Information given in [7–10] that is relevant for this study is published for the first time in the context of a reviewed journal paper here. The information is complemented by detailed studies of the damage behavior and its dependence on the grade of deformation. The influence of cold rolling on pore structure and specific flow resistivity compared to the change of mechanical properties of porous aluminum are shown. The results are analyzed to identify reasonable degrees of deformation for the fabrication of porous trailing edges. It must be pointed out that due to cold rolling, porosity and pore size decrease and consequently specific flow resistivity increases. The specific flow resistivity has a major influence on the reduction of trailing edge noise [4–6]. It is a main goal to produce material with specific flow resistivity similar to PA 80-110 which was used by Herr et al. [6]. Thus, it is reasonable to use material with greater pores and low specific flow resistivity for cold rolling. The mechanical properties of the cold-rolled material are then compared to those of PA 80-110 as received (which was used by Herr et al. [6]). In this study, PA 200-250 was selected for the rolling experiments. Based on the results, first experimental trailing edges made from cold-rolled porous aluminum for verification in an acoustic wind tunnel are shown and characterized. In this context a new rolling technique for the production of graded porous material is introduced. It is demonstrated that the shortcomings of porous materials for low-noise trailing edge applications pointed out by Herr et al. [6] can be overcome using cold rolling. Furthermore, the results show that the material can be rolled to a certain extent without a negative impact on mechanical strength.

2. Materials and Methods

2.1. Material

The porous aluminum that was used is produced by casting a placeholder structure. The technique used by "Exxentis" is called salt infiltration technique. Molten aluminum is poured into a casting mold which is filled with sodium chloride particulates. After casting, the material is cut into plates and the sodium chloride is washed out of the material. The contact areas of particulates become the link between pores. The particulates themselves become pores. Thus, by using a different size of particulates the size of the link between pores and the pore size itself are adjusted. In so doing the grade of filtration is adjusted. The material is named after the grade of filtration. In this study material with a grade of filtration in the range of 200–250 µm and a material with 80–110 µm grade of filtration was used. They are called PA 200-250 and PA 80-110 in the following. Typically, the material is made out of casting alloy AlSi7Mg, but other alloys are offered as well. For the experiments, material made out of technically pure aluminum A85 according to GOST (The Russian federal agency for technical regulation and metrology) was used, as it provides a high formability during cold rolling. The dimension of the received material was 500 mm × 300 mm × 20 mm. The plates were cut into smaller samples using a band saw and rolled subsequently.

Herr et al. [6] request a porous material with specific flow resistivity similar to the PA 80-110 they used. To achieve this, rolling experiments have been performed using PA 200-250. It provides a low specific flow resistivity compared to PA 80-110. As a result of cold rolling, specific flow resistivity increases. Mechanical testing and structural analysis have been performed with PA 80-110 and PA 200-250. Note, that the material used for the wind tunnel experiments by Herr et al. [6] was made out of the casting alloy AlSi7Mg.

2.2. Rolling Experiments

There were two rolling mills used in this study. The parameters of both are compared in Table 1.

Table 1. Parameters of rolling mill A (RMA) and the optimized rolling mill (RMB).

ParameterRolling Mill	RMA	RMB
Force F_{max}	600 kN	400 kN
Roll diameter D	250 mm	200 mm
Roll width W	250 mm	200 mm
Rolling speed	416 mm/s	5–50 mm/s
Adaptive gap between rolls	no	yes
Hydraulically operated pull out table	no	yes

The structural and mechanical characterization was done with samples rolled with rolling mill A (RMA). The finishing thickness after rolling was 90%, 80%, 70%, 60%, 50%, 40%, 30% and 25% of the initial thickness. Those values are equivalent to a true strain of −0.11, −0.22, −0.36, −0.51, −0.69, −0.92, −1.20 and −1.39. Due to the high rolling speed of RMA, a small reduction per pass of 0.2 mm had to be used, to prevent the samples from bending. Additionally, each pass consisted of rolling each sample four times, namely forwards and backwards, respectively, from the top and the bottom sides.

An optimization of the rolling process based on the research with samples rolled with RMA led to a specialized rolling mill system, namely rolling mill B. RMB provides an adaptive gap between rolls during the rolling process as well as a hydraulically operated pull out table. In this study, RMB was only used for the production of graded porous material. The porous material is restrained onto the pull-out table which gives accurate information about the position of the sample in relation to the gap between rolls. A closed-loop control allows adjusting the gap between rolls as a function of the position of the sample. For the graded experimental trailing edges, the material was rolled in five passes. The sample was rolled differently in three areas per pass. In the first area, rolling started with a small reduction per pass. In the second area, a linear gradient was rolled into the material. Hence, the third area had a major but constant reduction per pass. Each pass itself consisted of several steps. First, the gap between rolls opens up to a value >20 mm and the material is inserted into the gap. Second, the gap is closed until the reduction per pass for the first area is reached. Third, the rolls start to rotate, and the pull-out table moves into the direction of rolling, pulling the sample with a small, constant tension. Still, the movement of the sample is determined by the rolling speed. When the starting position for area two is reached, the gap between rolls closes while the rolls and the table are moving, thus, rolling a linear gradient. At the starting point of area three, the gap between rolls is kept at a constant value until the sample left the gap. Subsequently, the process starts with the first step again. Figure 1 shows the cross section of the geometry that is rolled. The corresponding thickness of different areas for each pass is shown in Table 2. The number of areas can be enlarged by using additional supporting points. In this way, different linear gradients can be rolled into the material. By using the supporting points, it is also possible to roll a curve-like shape into the material.

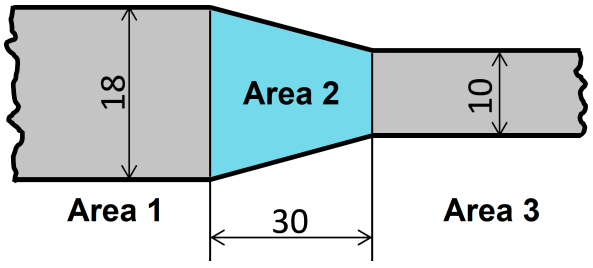

Figure 1. Cross section of graded rolled sample, different areas are marked.

Table 2. Gap between rolls in mm during each pass for each area.

Number of Pass	Area 1/mm	Area 2 (30 mm) Linear Gradient/mm→mm	Area 3/mm
1	19.60	19.60→17.40	17.40
2	19.21	19.21→15.13	15.13
3	18.82	18.82→13.17	13.17
4	18.45	18.45→11.45	11.45
5	18.00	18.00→10.00	10.00

2.3. Material Characterization

The material characterization was conducted using a CT scanner (GE nanotoms, GE Sensing & Inspection Technologies GmbH, Wunstorf, Germany) with a minimum voxel size of V = 0.5 µm. The voxel size used for the scans in this study varied from $V \approx 6$ µm to $V \approx 17$ µm due to different size of the samples. The pore structure was analyzed by applying a line segmentation technique to binarized cross-sectional image stacks of ten images each. The image stacks were extracted out of three-dimensional CT reconstructions of cold-rolled samples. Three different orientations with respect to the rolling process have been analyzed. Figure 2 illustrates the planes that were analyzed. The analyzed planes are named with respect to the application of the porous material as a trailing edge. The red image stack is called perpendicular, as the size of pore channels that are oriented perpendicular to the direction of flow over the aircraft's wing are determined with this image stack. Thus, the blue image stack is named lengthwise, as the pore channels that are to be measured are in the direction of flow referring to the flow of air over an aircraft's wing. Consequently, the green image stack is called transverse, as the pore channels are transverse to the direction of the air flow. The line segmentation technique was successfully applied to different porous materials [11–13]. This method provides a mean pore size and a mean ligament size, by measuring the mean length in black areas (pores) and white areas (material/ligaments) along each line of a pattern of lines with a given interval. This pattern of lines is then rotated 180° by steps of 1°, giving the mean length of pores and ligaments for each angle. The results can be shown in structural ellipses, where the mean length is plotted as a function of the angle. Due to the mirror symmetry of the line segmentation technique the result for each angle is plotted twice, namely at the angle that was measured as well as the angle +180°. Typical structural ellipses are shown in the following. It is necessary to point out, that the mean pore size given by this method is not the actual pore size as it is calculated by taking the mean of pores (former particulates) and the connection between pores (former area of contact between particulates). Thus, the values are not the same as the grade of filtration used by "Exxentis". By measuring the material as received as well, the values provide the possibility to describe the development of the pore structure during cold rolling. The porosity of the material was determined with three-dimensional CT reconstructions using VG Studio Max 2.1 by VolumeGraphics (Heidelberg, Germany).

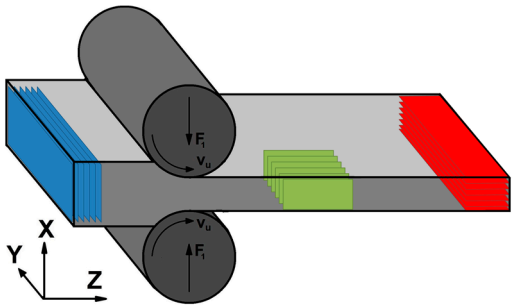

Figure 2. Orientation of cross-sectional image stacks with respect to the rolling process; red = perpendicular; blue = lengthwise; green = transverse.

For the characterization of the porosity of the experimental trailing edges, they were subdivided into six different Regions of Interest (ROI). The porosity was then determined for each Region of Interest. This is shown in Figure 3. As can be seen in Figure 3, the volume of the regions is decreasing (from ROI 6 to 1), because the material gets thinner. However, there is enough material to determine a reliable porosity value based on the analyzed volumes.

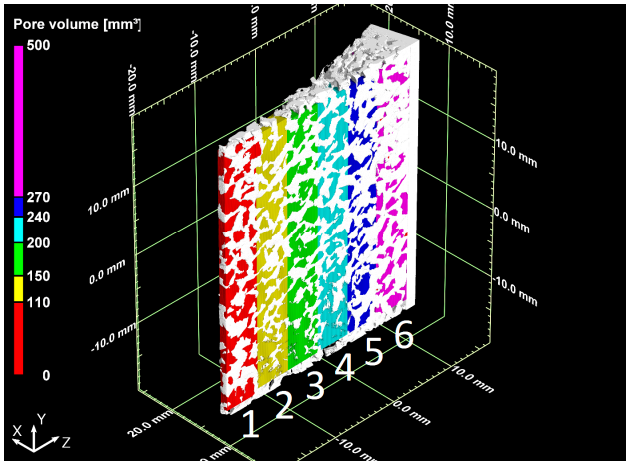

Figure 3. Experimental trailing edge, subdivided into six Regions of Interest for the measurement of porosity (material: white, pore volume: color coded).

As mechanical testing, tensile tests were performed with samples designed according to DIN 50125 form E. The samples were cut with a milling machine even though material is forced into the open porosity during the process. The influence on the results of mechanical testing due to the altered surface is insignificant [14,15]. The material was fixed in the tensile testing machine using self-tightening clamping jaws. A modification of the dimensions of Form E (DIN 50125) was made to allow CT measurements of the entire measuring zone of the tensile test samples ($L_0 \times b_0 \times a_0$). A schematic diagram of the sample is shown in Figure 4. The associated dimensions are given in Table 3.

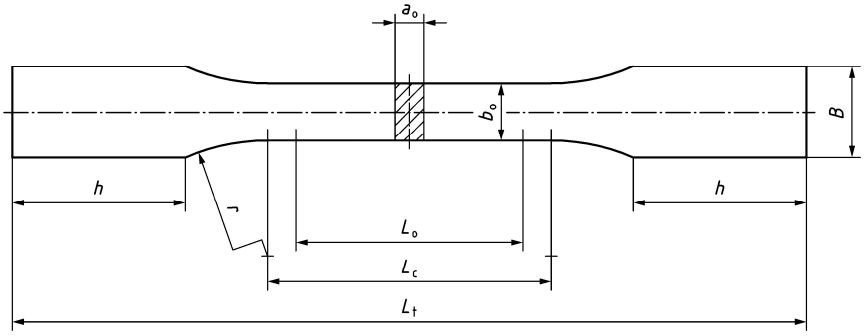

Figure 4. Schematic Diagram of tensile test samples according to DIN 50125.

Table 3. Dimensions of tensile test samples.

Parameter According to DIN 50125	a_0	b_0	B	h	L_0	L_c	L_t	r
Value/mm	8	12	18	40	30	36	140	12

Besides continuous tensile testing, discontinuous tensile tests have been performed to examine the damage behavior of the material and the influence of cold rolling on the damage behavior. The samples

were repeatedly dilated with small plastic strains. After every step of elongation, the samples were scanned and analyzed using CT. The samples were marked with copper strips to be able to analyze the same volume of the sample each time. This way of analyzing the damage behavior has been successfully performed for sintered fiber felts by Lippitz et al. [16]. Here, it has been performed for material as received and for material with a thickness reduction $\Delta t/t_0$ of 20% and 50%.

The noise reduction potential of porous trailing edges is based upon the connection between pressure- and suction side of a wing. The connection allows pressure equalization of turbulent flow, leading to significant reduction of noise generated at the end of the trailing edge. Thus, specific flow resistivity, particularly in the perpendicular direction, is an important parameter characterizing the aeroacoustic behavior [6].

The flow resistivity measurements were conducted at the Institute for Engineering Design—TU Braunschweig and at the Physikalisch-Technische Bundesanstalt (PTB, National Metrology Institute) in Brunswick. The samples have been produced with rolling mill A (RMA). Three main orientations with respect to the rolling process (Figure 2) have been characterized. The alternating air flow method (according to Method B DIN EN 29035) with an uncertainty of 14% [17] was used. The material as received and after cold rolling was wire-cut into four square plates of 60 mm edge length each using electrical discharge machining to obtain samples with open porosity. The thickness was given by the degree of deformation. As the sample sizes differ from the instrument specimen mount, an adapter was used to fix the samples. Surfaces parallel to the direction of measurement were sealed with adhesive tape. Gaps between the specimen mount and the sample were sealed with modelling clay. The measured values of difference in pressure were put into relation to the sample geometry according to DIN EN 29035. Thus, a specific flow resistivity which is comparable for different samples was obtained.

Another parameter for the characterization of porous materials is the tortuosity. Even though the tortuosity α_∞ is not measured or calculated in this study, it is used to explain changes in specific flow resistivity. That is why the concept of tortuosity according to Allard et al. [18] is briefly described in the following. The tortuosity α_∞ is defined as [18]:

$$\alpha_\infty = 1/\cos^2\varphi \tag{1}$$

with

$$\cos\varphi = \frac{d}{l} \tag{2}$$

This is exemplified shown in Figure 5 for a simple porous material (one straight and continuous pore). d is the thickness of material and l the length of a pore. The concept can be used for complex materials, like porous aluminum, as well [18]. The tortuosity α_∞ is a measure for the tortuosity of "channels" through the open porous material.

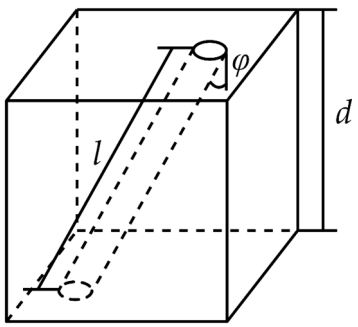

Figure 5. Schema of a simple porous material.

3. Results and Discussion

Results regarding the porous structure, flow resistivity and mechanical behavior are shown. The findings are used to deduce reasonable degrees of deformation for the production of low-noise trailing edges. This information is used for the production of experimental trailing edges, which are characterized and shown. They have partly been produced using a new cold rolling technique for the production of graded porous material. The technique itself has been described in the Materials and Methods section.

3.1. Porous Structure

An important point for the usage of porous material as low-noise trailing edge is the openness of porosity. Figure 6 shows three-dimensional reconstructions of cold-rolled PA 200-250 after different thickness reductions during rolling. Displayed are the pores, which are color coded according to their size. For the undeformed material one large pore (colored in red) can be seen. It is existent up to a true strain of -1.20 ($\Delta t/t_0 = 70\%$). The higher the deformation is, the more minor pores (colored in blue) can be seen. These pores are disconnected from the main pore volume. They are in the boundary areas of the analyzed volumes. Considering their surroundings, they are likely to be connected to the main pore volume as well, but cut off due to the restriction of the analyzed area (Figure 6a–e). Consequently, open porosity is kept to a high level of deformation ($\Delta t/t_0 = 70\%$) for PA 200-250.

At a true strain of -1.39 ($\Delta t/t_0 = 75\%$), minor pores (colored in blue) can be seen in the center of the analyzed volume (Figure 6f). The pores are not connected and do not contribute to the materials permeability. The former main pore volume is split up into smaller pore volumes (colored in red, light blue and turquois). Thus, openness of porosity is highly limited for thickness reductions more than 70%. Similar results for the porosity are obtained for cold-rolled PA 80-110. A thickness reduction $\Delta t/t_0$ of 70% led to predominantly closed pores for PA 80-110 [7]. Besides the openness of porosity, Figure 6f shows that nonhomogeneous plastic flow occurs for high degrees of deformation, as there are small closed pore volumes (colored in blue) as well as bigger pore volumes (colored in red, light blue and turquois) randomly scattered over the analyzed volume.

With respect to the shortcomings of porous materials for low-noise trailing edge applications found by Herr et al. [6], the analyzation of openness of porosity (Figure 6) disclose the first limitations for the degree of deformation during cold rolling. On the one hand, a thickness reduction greater than $\Delta t/t_0 = 70\%$ is not suitable for constantly cold-rolled material (no gradient in thickness reduction). The material is almost non-permeable, thus the favored aeroacoustic behavior cannot occur. On the other hand, a thickness reduction about $\Delta t/t_0 = 75\%$ is very well suited for low-noise trailing edge applications, if it is used for the production of graded porous material. A smooth transition from material with closed pores (nonpermeable, $\Delta t/t_0 = 75\%$) to open porous material (fully permeable, $\Delta t/t_0 << 75\%$) can be achieved.

According to the manufacturer, the porosity of both, PA 200-250 and PA 80-110, is essentially the same varying from 50 to 55%. Thus, it is not surprising that the results regarding the openness of the pores are similar. CT Scans disclosed that the porosity of the received material was slightly higher, i.e., 57% (PA 80-110, [19]) or 59% (PA 200-250). Table 4 shows the porosity Φ of samples out of PA 200-250 and PA 80-110 before and after cold rolling at different degrees of deformation. Considering the initial porosity of 59% of PA 200-250 a porosity of 18% has to result if the material is compressed with 50% thickness reduction $\Delta t/t_0$ without changing dimensions in other directions. However, measurements show the reduction of porosity to a value of 33%. During cold rolling the material is compressed in the x-direction but lengthened in the direction of rolling (z-direction). Spreading occurs in the direction transverse to the direction of rolling (y-direction). For a thickness reduction $\Delta t/t_0$ of 50%, lengthening was about 20%, whereas spreading was about 4%. Taking this into account, a porosity of 34% has to result. This is in good agreement with the measured value of 33% porosity. Thus, the porosity does not decrease like thickness reduction increases.

Table 4. Porosity of PA 80-110 (alloy A85) [19] and PA 200-250 (alloy A85) before and after cold rolling.

Material | $\Delta t/t_0$/%	0	10	20	30	40	50	60
$\Phi/1$ of PA 80-110	0.57	0.55	0.53	0.49	0.35	0.27	0.20
$\Phi/1$ of PA 200-250	0.59	0.56	0.52	0.47	0.41	0.33	0.23

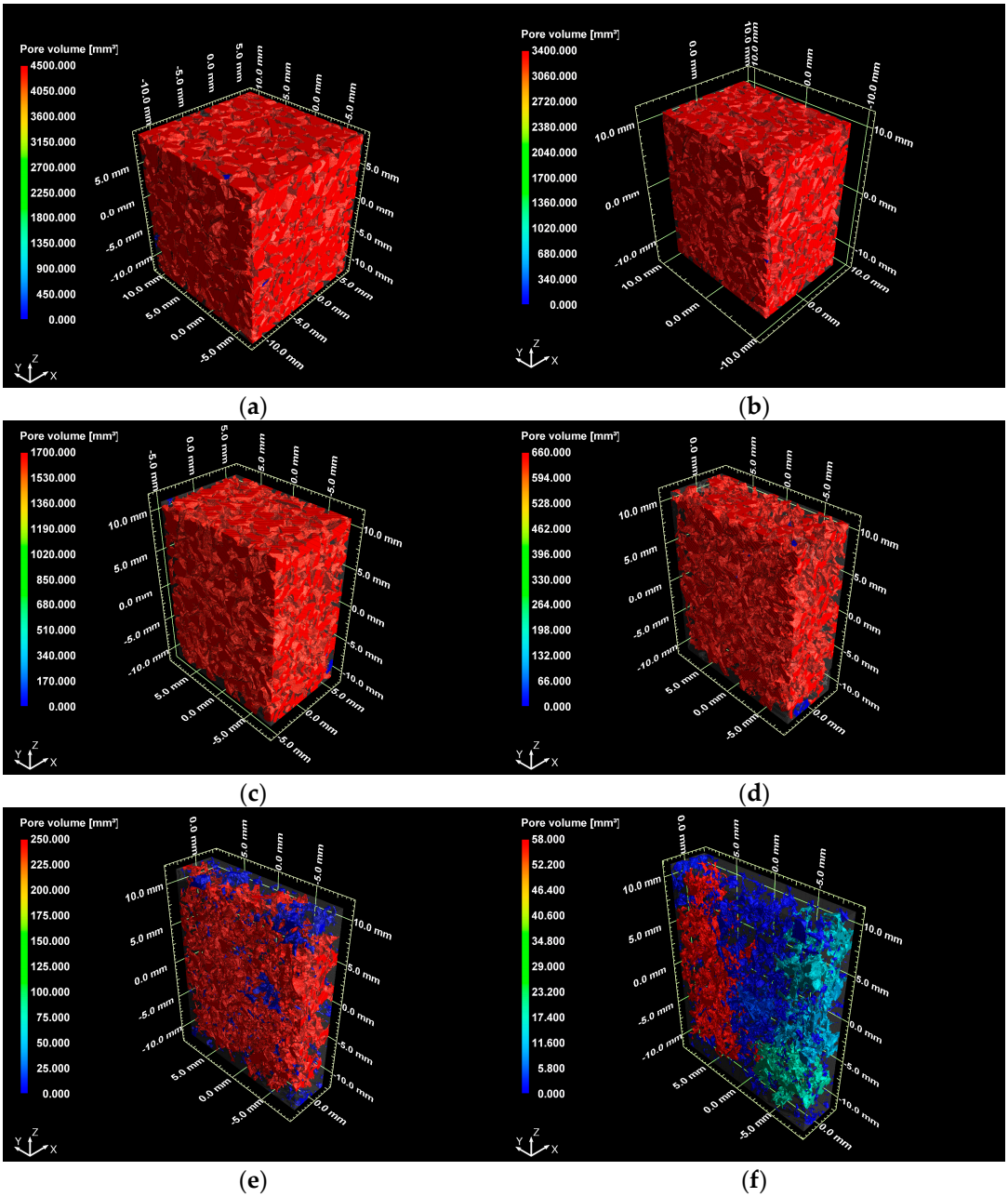

Figure 6. PA 200-250 at different degrees of deformation (material: transparent, pore volume: color coded) (**a**) before cold rolling; (**b**) $\Delta t/t_0$ = 20%; (**c**) $\Delta t/t_0$ = 40%; (**d**) $\Delta t/t_0$ = 60%; (**e**) $\Delta t/t_0$ = 70%; (**f**) $\Delta t/t_0$ = 75%.

Lengthening of pores in the direction of rolling can be shown with the line segmentation technique. The results are plotted in structural ellipses in Figure 7. The mean pore size along the pattern of lines is given from 0° to 359° with respect to the plane that was analyzed (Figure 2). With an increase of the degree of deformation, the mean pore size decreases in every direction. This suits the results of

a decreasing porosity. Furthermore it can be seen that a major reduction of the pore size occurs in the direction of the gap between rolls (90° respectively 270° Figure 7b,c), whereas the reduction is less in the direction of rolling and in the direction of the roll width (0° respectively 180° Figure 7b,c), which results in ellipses elongated in the horizontal direction (Figure 7b,c).

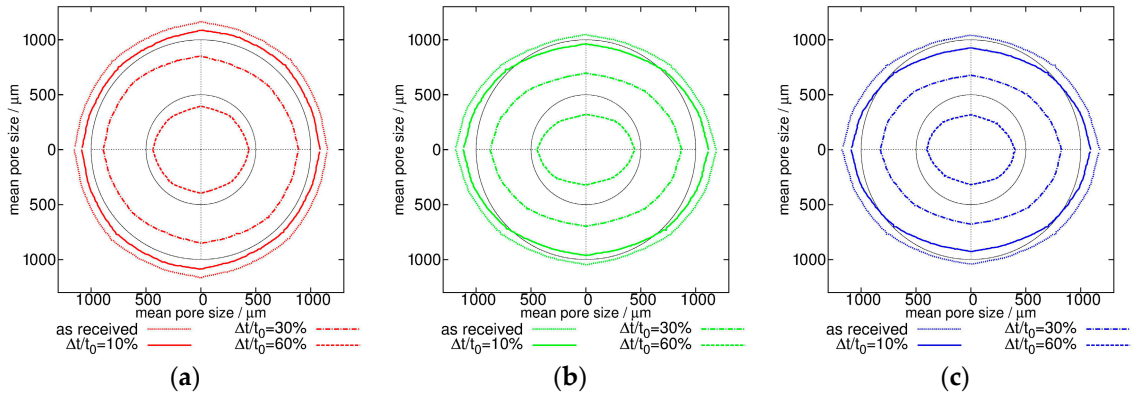

Figure 7. Structural ellipses of PA 200-250 for the material as received and for different degrees of deformation: (**a**) perpendicular; (**b**) transverse; (**c**) lengthwise [9].

The anisotropic pore shape is a result of compression as well as lengthening of pores in the direction of rolling, which can be seen in Figure 7a. In this plane, the effect of compression of pores is the same for every angle. Nevertheless, the plot shows a slightly elongated ellipse in the direction of rolling (horizontal). This is a result of lengthening of the samples in the direction of rolling during the rolling process. However, the difference in macroscopic deformation of the samples and the microscopic deformation of pores is remarkable. As mentioned before, lengthening of rolled plates at a thickness reduction $\Delta t/t_0$ of 50% is around 20% and spreading is about 4%, whereas the microscopic deformation of pores shows an overall decrease of pore size. The indentation of ligaments into pores during rolling is an explanation for the measured, overall decrease of pore size. This indentation leads to smaller pores but as well to an increase in tortuosity. The higher the tortuosity of the material is, the smaller are the pores measured with the line segmentation technique, as it gives a mean value of pores and pore channels for each angle. With respect to the aforementioned shortcomings of porous materials for the application as low-noise trailing edges it is expected that anisotropy of the pore shape needs to be further increased to affect the aeroacoustics of the material.

3.2. Flow Resistivity

As described in the Materials and Methods section, the alternating air flow method was used to determine the specific flow resistivity r. The uncertainty of the method according to DIN EN 29035 is 14%. In the following, mean values of r obtained on four samples along with standard deviations are shown for each degree of deformation. Note that the uncertainty of 14% is not taken into account for the given values.

The correlation between the specific flow resistivity and the degree of deformation is shown in Figure 8 for different directions with respect to the rolling process. The material, as received, has a similar specific flow resistivity in every direction with low scattering. The measurements support the results of the structural characterization as they show an increasing anisotropic behavior of the material for an increasing degree of deformation. In this context, an increasing anisotropic behavior means a rising difference in flow resistivity values between the different directions. The specific flow resistivity is being highest in the direction perpendicular to the rolled surface (Figure 8b). However, the evolution of the specific flow resistivity cannot be entirely explained by the measurements of the mean length of pores, as the specific flow resistivity is highest in the direction with biggest pores

(compare: Figures 7a and 8b). This can only be explained due to an increased tortuosity in the perpendicular direction compared to the other directions. This effect intensifies with an increase in the degree of deformation. Furthermore, scattering between the values is increasing, the higher the deformation is. Scattering of the flow resistivity values might be due to nonhomogeneous plastic flow during cold rolling, changing the stochastic structure of the material. For high degrees of deformation this can be seen in Figure 6e,f. There are areas with small, closed pores whereas other areas still consist of bigger pore volumes (colored red, light blue and turquois in Figure 6f). It can be assumed that there are areas with nonhomogeneous deformation at lower degrees of deformation as well. Those would not be completely closed, but have a higher specific flow resistivity than the rest of the sample. Depending on the amount of such areas, the specific flow resistivity of the entire sample is more or less influenced. It needs to be pointed out, that this is not a result of damaging but due to the stochastic structure of the material. The analyzation of the damage behavior supports this reasoning and is shown in the next section.

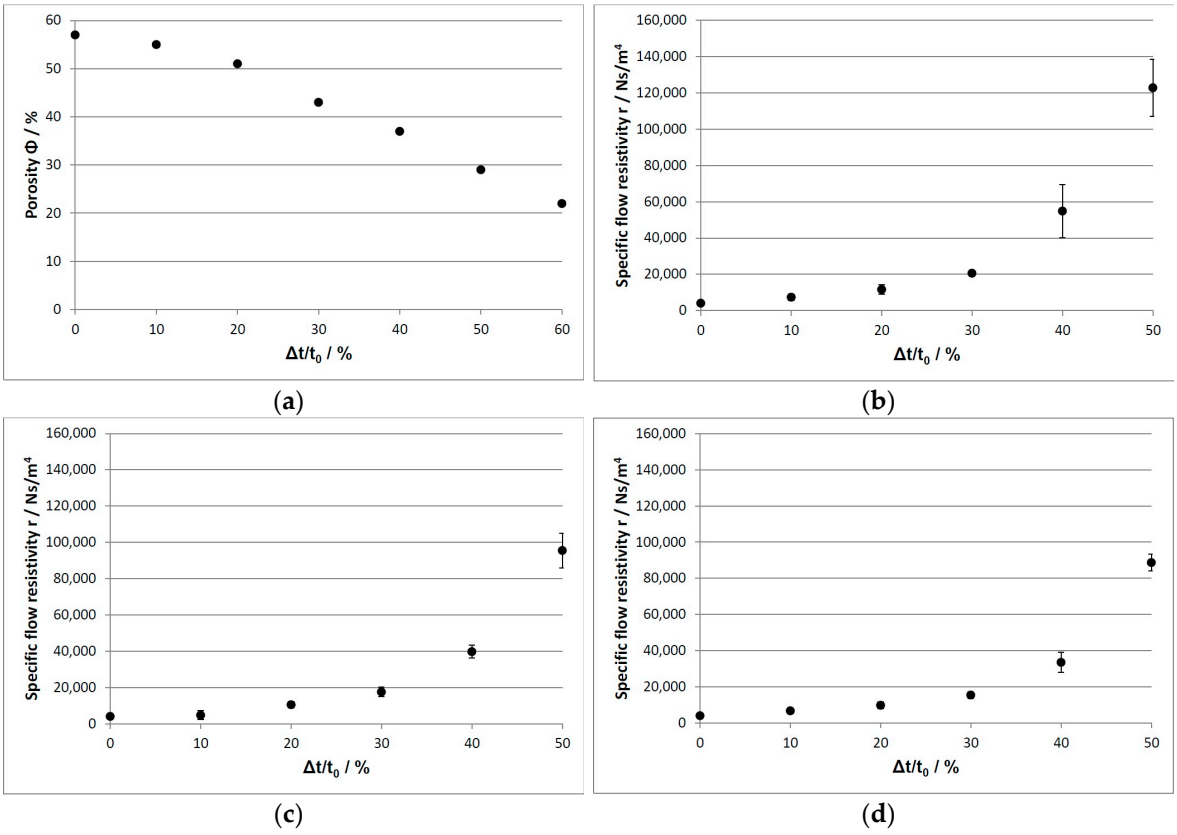

Figure 8. Porosity and specific flow resistivity *r* of PA 200-250 at different degrees of deformation (**a**) porosity; (**b**) *r*, perpendicular; (**c**) *r*, transverse; (**d**) *r*, lengthwise. [8].

Note, that the undeformed PA 80-110 (made out of casting alloy AlSi7Mg) which was used for the wind tunnel experiments by Herr et al. [6] has a specific flow resistivity of 145,500 $\pm$ 10.7 Ns/m^4 in the perpendicular direction (uncertainty of 14% not taken into account). As the aeroacoustics performance of the experimental trailing edge in [6] is promising, a material with similar or overlapping (with respect to graded material) flow resistivity in the perpendicular direction but elongated pores had to be produced. As can be seen in Figure 8b, cold-rolled PA 200-250 with an initial thickness of 20 mm and a thickness reduction of 50% meets the required range of flow resistivity in the perpendicular direction.

3.3. Mechanical Behavior

The mechanical behavior was characterized through tensile tests. On one hand, tensile tests were performed to determine mechanical parameters like the yield strength. The yield strength is shown in the following as a measure of mechanical strength of the material. On the other hand, discontinuous tensile tests were performed to analyze the damage behavior of the material, as well as the influence of cold rolling on the damage behavior. The results for the damage behavior are presented at the end of this chapter.

The results of mechanical testing of different directions with respect to the rolling process (compare Figure 2) are shown in Figure 9. Tests have been conducted into the *z*-direction (Figure 9a) and in the *y*-direction (Figure 9b). The *x*-direction has not been analyzed as the material thickness is too thin to produce tensile test samples. For the analyzed directions the development of the yield strength $R_{p0.2}$ is similar. A smaller value, compared to the initial state, results for a thickness reduction of 10%. With further reduction of thickness, the yield strength is increasing, but showing scattering for high degrees of deformation ($\Delta t/t_0$ = 50–60%). Scattering occurs for small degrees of deformation as well (Figure 9a for $\Delta t/t_0$ = 30% and Figure 9b for $\Delta t/t_0$ = 10%) but it is more pronounced for high degrees of deformation. This might be a result of the dimensions of the samples combined with the nonhomogeneous plastic flow during cold rolling. Small differences in the initial structure can reduce the load bearing cross section during tensile testing, leading to scattering of values between different samples independent of the degree of deformation. For high degrees of deformation, the aforementioned nonhomogeneous plastic flow during cold rolling (Figure 6) leads to additional heterogeneity of the material. Depending on where the measurement range of the tensile test sample is with respect to the rolled material and whether it includes a particular region that has not been densified as much as the rest of the sample, the measured yield strength may scatter between different samples. This is consistent with the results that were obtained for the flow resistivity measurements, where scattering increased at high degrees of deformation.

The overall increase of the yield strength can be explained by decreasing porosity during cold rolling. The size of the tensile test sample is the same, but the amount of load-bearing material with respect to the cross section A of the tensile testing samples is increasing. That is why the yield strength obtained from the tensile test, as well as a corrected yield strength $R_{p0.2}{}^*$ is plotted in Figure 9. The corrected yield strength is calculated using Equation (3):

$$R_{p0.2}{}^* = R_{p0.2} \cdot (A/A^*) \tag{3}$$

$$A^* = A\,(1 - \Phi) \tag{4}$$

The corrected cross section A^*, which is used to determine $R_{p0.2}{}^*$, is calculated according to Equation (4) using the porosity values Φ for PA 200-250 displayed in Figure 8a. The corrected yield strength allows comparing the stress carried by the ligaments. For this reason, the corrected yield strength is always greater than the yield strength itself.

Analyzing the corrected yield strength, a steady increase in the yield strength of the material cannot be deducted. Thus, strengthening of the samples can only be explained by the increase of load-bearing material because of decreasing porosity. However, as the corrected yield strength stays essentially constant over the entire range of deformation, there is also no weakening due to cold rolling. This demonstrates that large degrees of deformation are feasible for the production of low-noise trailing edges without undue deterioration of mechanical properties. In this context, it is worthwhile to compare cold-rolled PA 200-250 with PA 80-110 as received made of A85. After a thickness reduction of $\Delta t/t_0$ = 50%, the former material exhibits a similar, advantageous specific flow resistivity as the latter (compare with Section 3.2. Flow resistivity). However, the yield strength of the former material is 13.6 $\pm$ 2.9 MPa (*z*-direction) and 16.8 $\pm$ 2.6 MPa (*y*-direction) (see Figure 9) compared to 5.11 $\pm$ 0.18 MPa for the latter. This demonstrates that cold rolling of porous materials is a viable method to tailor

properties in a beneficial fashion. The analysis of the damage behavior, which is presented in the following, upholds this conclusion.

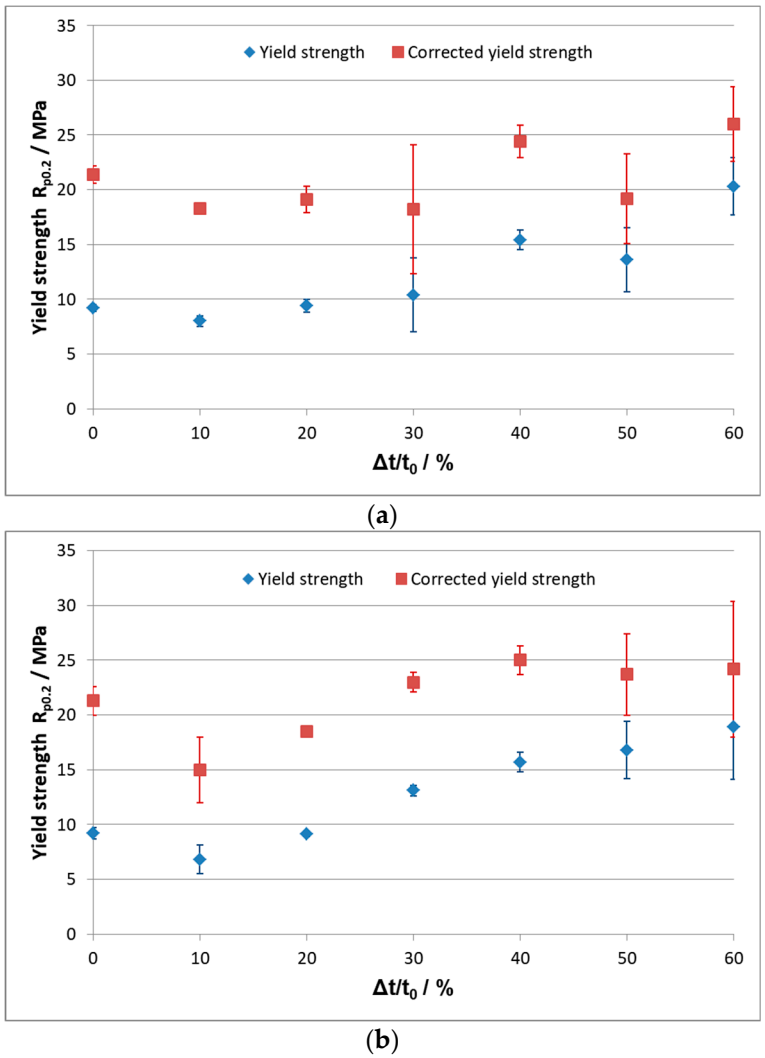

Figure 9. Yield strength $R_{p0.2}$ of PA 200-250 at different degrees of deformation (**a**) loading in the direction of rolling (*z*-direction); (**b**) loading in the direction of roll width (*y*-direction). [8,9].

Research on the damage behavior based on discontinuous tensile tests show that the material starts to collapse in areas where major pores and small ligaments are. Thus, collapsing starts on the short side of the sample, because there is an increased possibility of a major, end-to-end pore connecting both surfaces of the material. Those pores are shown in Figure 10a,b, Figures 11a and 12a, marked with a green line. Note that all the figures show the samples from the short side. As the load bearing cross section is reduced, further collapsing proceeds from those areas. This effect was obtained for the material as received, as well as for both kinds of cold-rolled material. This is shown in Figure 10c–h for the material as received and for cold-rolled material with a thickness reduction $\Delta t/t_0$ of 20% in Figure 10c–h and for material with a thickness reduction $\Delta t/t_0$ of 50% in Figure 11c–h.

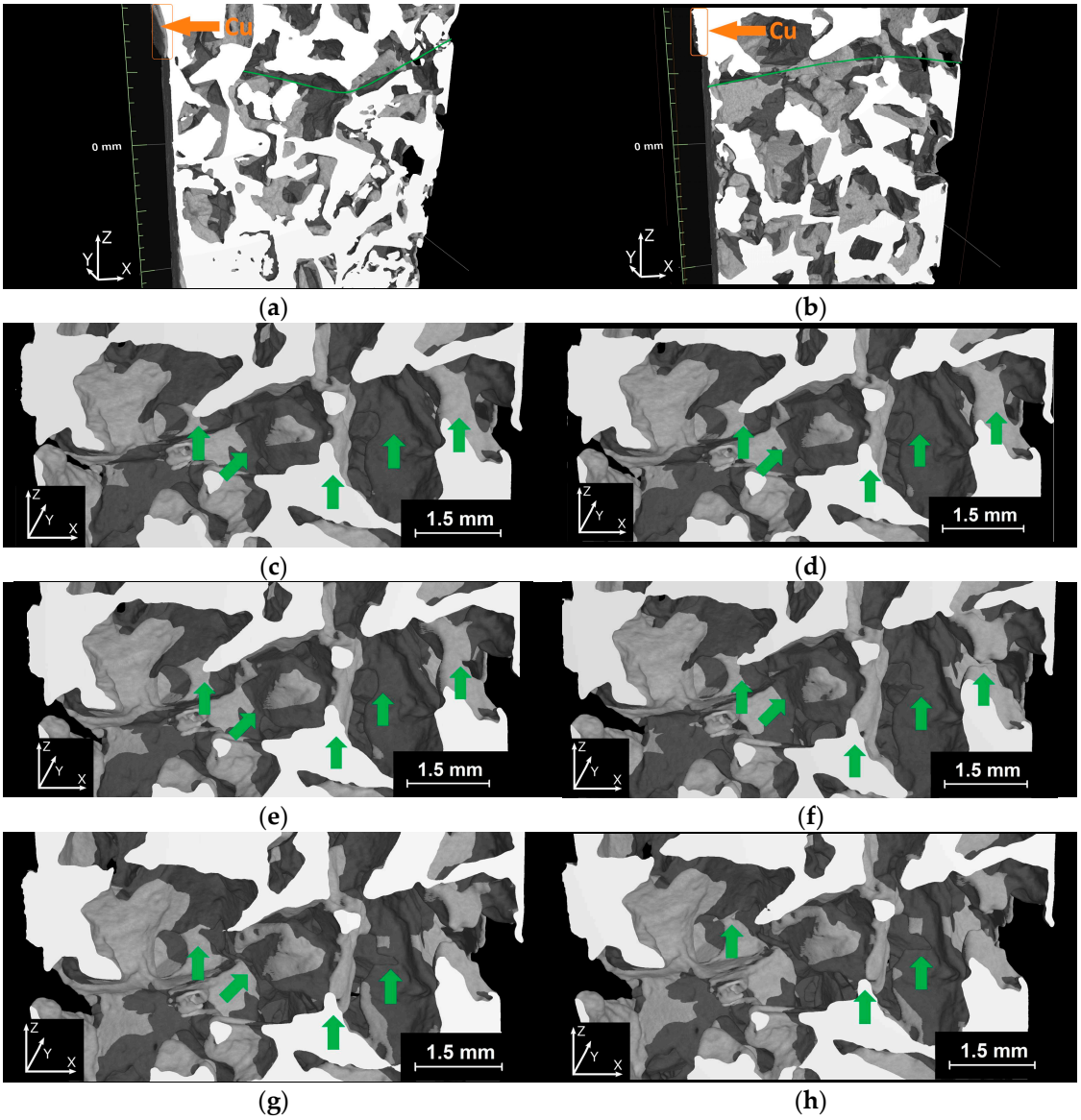

Figure 10. 3D CT reconstructions of tensile test sample (z-direction: direction of stress) out of PA 200-250 as received, cross sections under ($y = -0.25$ to -1 mm) the samples surface ($y = 0$) at different plastic strains ε_{pl} (material: white) (**a**) major end-to-end pore $\varepsilon_{pl} = 0\%$ ($y = -0.25$ mm); (**b**) major end-to-end pore $\varepsilon_{pl} = 0\%$ ($y = -0.75$ mm); (**c**) $\varepsilon_{pl} = 2.31\%$ ($y \approx -1$ mm); (**d**) $\varepsilon_{pl} = 2.81\%$ ($y \approx -1$ mm); (**e**) $\varepsilon_{pl} = 3.31\%$ ($y \approx -1$ mm); (**f**) $\varepsilon_{pl} = 3.81\%$ ($y \approx -1$ mm); (**g**) $\varepsilon_{pl} = 4.31\%$ ($y \approx -1$ mm); (**h**) $\varepsilon_{pl} = 4.81\%$ ($y \approx -1$ mm).

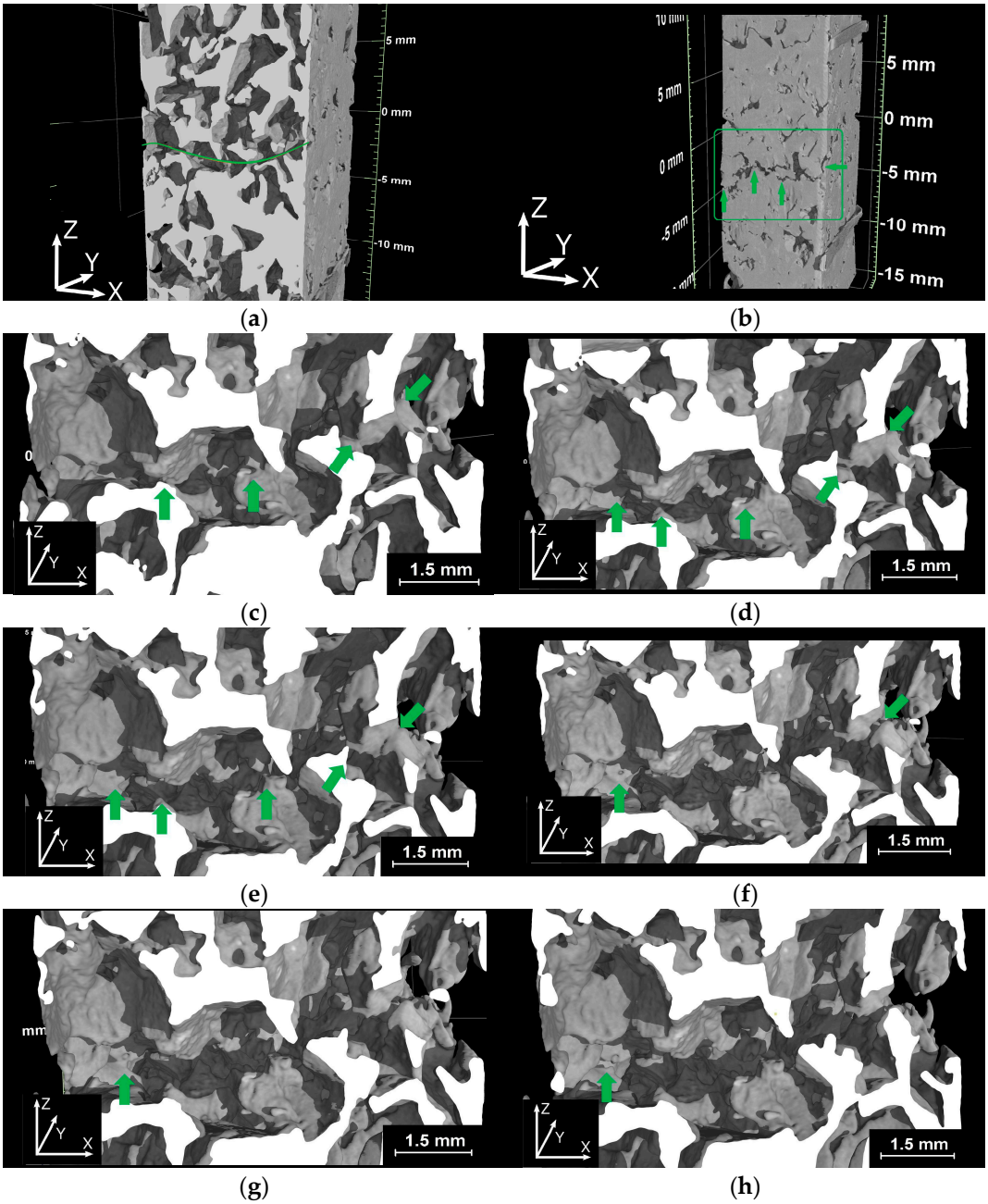

Figure 11. 3D CT reconstructions of tensile test sample (z-direction: direction of stress) out of PA 200-250 $\Delta t/t_0$ = 20%, cross sections under (y = −0.25 to −0.5 mm) the samples surface (y = 0) at different plastic strains ε_{pl} (material: white) (**a**) major end-to-end pore ε_{pl} = 0% (y = −0.5 mm); (**b**) path of crack at ε_{pl} = 2.3% (y = −0 mm); (**c**) ε_{pl} = 2.62% ($y \approx -0.25$ mm); (**d**) ε_{pl} = 3.6% ($y \approx -0.25$ mm); (**e**) ε_{pl} = 4.6% ($y \approx -0.25$ mm); (**f**) ε_{pl} = 5.1% ($y \approx -0.25$ mm); (**g**) ε_{pl} = 5.6% ($y \approx -0.25$ mm); (**h**) ε_{pl} = 6.1% ($y \approx -0.25$ mm).

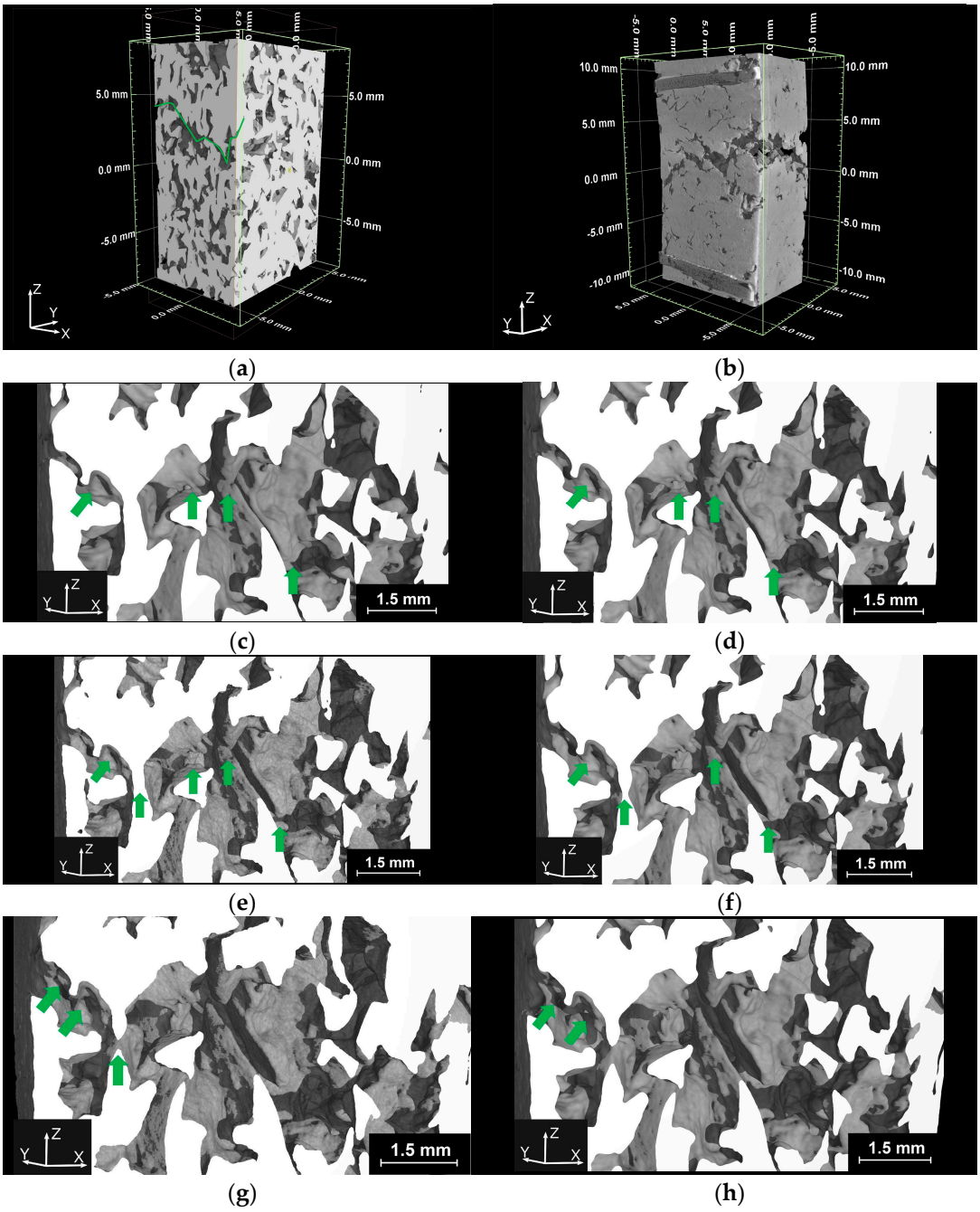

Figure 12. 3D CT reconstructions of tensile test sample (*z*-direction: direction of stress) out of PA 200-250 $\Delta t/t_0$ = 50%, cross sections under (y = −0.25 to −0.5 mm) the samples surface (y = 0) at different plastic strains ε_{pl} (material: white) (**a**) major end-to-end pore ε_{pl} = 0% (y = −0.5 mm); (**b**) path of crack at ε_{pl} = 5.9% (y = −0 mm); (**c**) ε_{pl} = 0.92% ($y \approx -0.25$ mm); (**d**) ε_{pl} = 1.18% ($y \approx -0.25$ mm); (**e**) ε_{pl} = 1.49% ($y \approx -0.25$ mm); (**f**) ε_{pl} = 1.89% ($y \approx -0.25$ mm); (**g**) ε_{pl} = 2.29% ($y \approx -0.25$ mm); (**h**) ε_{pl} = 2.69% ($y \approx -0.25$ mm).

The major end-to-end pore found in the sample made out of PA 200-250 as received is displayed in Figure 10a,b. Figure 10a shows a cross section of the reconstructed volume of the sample with the first 0.25 mm of material (from the surface) hidden. On the left of the sample, a few ligaments can be seen. The ligaments on the left side of the sample, however, do not extend deep into the sample. They are no longer visible when cut at 0.75 mm below the sample's surface. In this cross section

(Figure 10b), an almost straight pore, or pore channel, over the entire width of the sample can be seen. Such large, continuous pores were found only in areas near the surface where crack propagation later on starts.

Figure 10c–h displays the major end-to-end pore of the tensile test sample made out of PA 200-250 as received for different plastic strains ε_{pl} during tensile testing. The green arrows mark ligaments that show a deformation or a constriction. With increasing deformation of the sample, some of the marked ligaments completely separate. The first ligament that fails completely is marked by the green arrow on the far right (Figure 10c–f). Note that the individual ligaments show a much greater deformation than the entire tensile test sample. However, due to a lack of fixed points, the deformation of a single ligament is difficult to determine. For a plastic strain of 0.5% of the entire sample, plastic strains of individual ligaments between 5% and 10% were determined on the basis of the images shown. It can also be seen that the crack path does not run straight through the material, but shows a jagged path, depending on the position of pores and ligaments. For the first ligament that separates, the crack path runs horizontally, whereas one ligament in the mid region of the sample (second arrow from the left in Figure 10c–g) is separated by an oblique tear. In addition, a ligament which is separated obliquely in the *yz*-direction can be seen directly at the cutting plane (third arrow from the left in Figure 10e–g).

The results for the sample made out of cold-rolled PA 200-250 with a thickness reduction $\Delta t/t_0$ of 20% are displayed in Figure 11a–h. Figure 11a shows the major end-to-end pore (green line), which was found below the surface (0.5 mm), in the area where crack propagation starts later on. The beginning of the crack path itself is shown in Figure 11b (green box marks the area; green arrows mark the crack). As mentioned in the Materials and Methods Section, the samples were cut out of the cold-rolled material by mechanical milling. Therefore, the surface of the samples was smeared with material. This can be seen in Figure 11b, as there are too few pores visible at the surface. The material that is smeared into pores during mechanical milling has no load bearing function. It shows no elongation and thus, small gaps open up during tensile testing, where the material has been smeared into the pores. Hence, areas with high plastic strain can be seen quite well at the sample surface. That is why the posterior crack path can be seen at a plastic strain ε_{pl} of 2.3% in Figure 11b, even though the ligaments within the sample in Figure 11c (ε_{pl} of 2.62%) show no constriction or failure.

The crack path of cold-rolled PA 200-250 with a thickness reduction $\Delta t/t_0$ of 20% itself shows essentially the same behavior as it was determined for the sample made out of PA 200-250 as received. This is displayed in Figure 11c–h. Like before, the green arrows mark ligaments that show a deformation, constriction or failure. Of particular interest is the ligament on the right side of the sample, which is marked by the outer right arrow. When the ligament, which is marked by the second arrow from the right, fails (Figure 11d–e), the other ligament seems to fail due to shearing (Figure 11d–f).

The results for the cold-rolled material with a thickness reduction $\Delta t/t_0$ of 50% are in good agreement with the previous results. Again, a large, continuous pore which extends deep into the sample (Figure 12a) was detected in the area of the posterior crack (Figure 12b). In contrast to the previous samples, it can be seen that the major end-to-end pore is much more tortuous. This is due to the densification of the material during cold rolling. Besides this difference, the material behaves analogous to the non-rolled and the less heavily rolled material when damaged during tensile testing. Figure 12c–h displays the crack growth within the material during tensile testing. As before, ligaments that show deformation, constriction or failure are marked with green arrows.

Since the cold-rolled samples show essentially the same damage behavior as the non-rolled material, it becomes clear that cold rolling has no negative influence on the damage behavior of the material. In addition, no damage due to cold rolling could be determined during the analysis of the samples. Therefore, large degrees of deformation are feasible for the production of low-noise trailing edges without undue deterioration of mechanical properties.

3.4. Experimental Low-noise Trailing Edges

Experimental trailing edges are wire cut out of the material by electrical discharge machining. They are shown and characterized by porosity measurements in the following. In Figure 13, a section of the experimental trailing edge analyzed in the acoustic wind tunnel by [6] is shown. The numbering of the Regions of Interest that has been shown in the Materials and Methods Section is shown in Figure 13a as well. This numbering is used in Table 5.

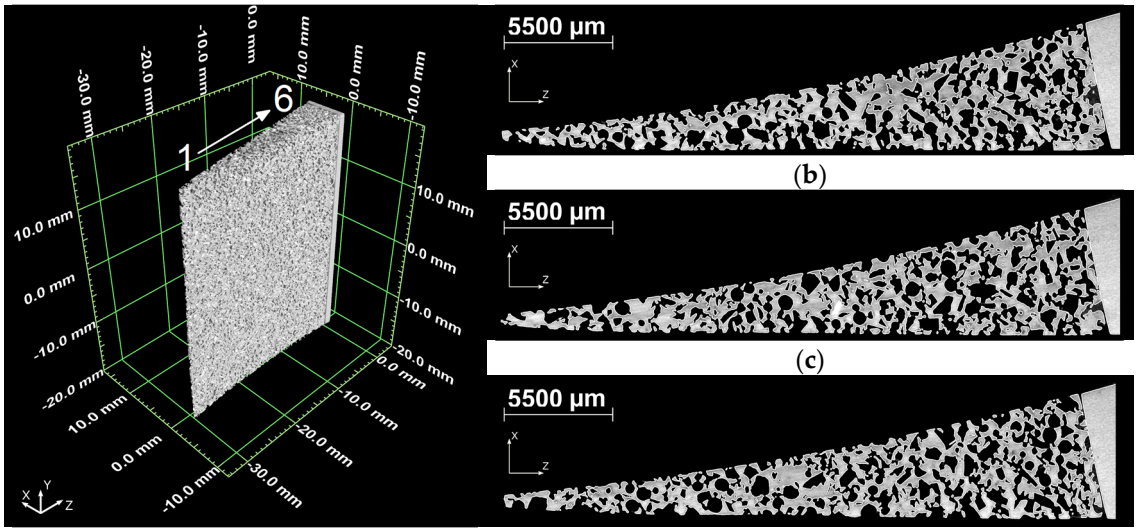

Figure 13. Section of an experimental trailing edge made of PA 80-110 (alloy AlSi7Mg) used by [6]: (**a**) reconstructed volume; (**b**) cross section at 10 mm (y-direction); (**c**) cross section at 0 mm (y-direction); (**d**) cross section at −10 mm (y-direction).

Table 5. Porosity Φ of experimental trailing edges, measured in Region 1–6.

Porosity Φ/1 of | No. of Region of Interest	**1**	**2**	**3**	**4**	**5**	**6**
PA 80-110 (AlSi7Mg) as received (used by [6]) (Figure 13)	0.53	0.53	0.54	0.53	0.53	0.53
PA 200-250 (A85) as received (Figure 14)	0.55	0.55	0.53	0.54	0.54	0.54
PA 200-250 (A85) $\Delta t/t_0$ = 50% (Figure 15)	0.25	0.29	0.33	0.32	0.33	0.31
graded PA 200-250 (A85) $\Delta t/t_0$ = 10–50% (Figure 16)	0.49	0.49	0.46	0.39	0.34	0.28

In Table 5 it can be seen, that the porosity for the materials as received is constant for all analyzed regions. For the sample made out of cold-rolled PA 200-250 with a thickness reduction $\Delta t/t_0$ of 50% Table 5 displays essentially constant porosity values except for region 1. Due to the geometry of the experimental trailing edges the analyzed volume for region 1 is comparatively small. The scattering of the value for region 1 can be explained well, considering the aforementioned nonhomogeneous plastic flow, particularly for high degrees of deformation. The porosity values of the other regions of the sample are in good agreement with the measured values of porosity in the section "Porous structure".

During cold rolling the surfaces of the samples experience a larger deformation than the material in the middle. This effect dominates for small degrees of deformation. This can be seen in Table 5 for the porosity values for the graded material (Figure 16). Regions 1 and 2 have the same porosity even though a linear gradient (compare Table 2) was rolled into the material. For regions 1 and 2 the thickness reduction is relatively small. Because the trailing edge is wire cut by electrical discharge machining out of the middle of a rolled plate, the more deformed, near-surface areas are cut off. For this reason, the specific flow resistivity of the experimental trailing edge might be a little smaller than the specific flow resistivity of the samples that were used for the flow resistivity measurements.

For regions with a major thickness reduction of 50%, the influence is insignificant. This can be seen for the cold-rolled material without a gradient in thickness reduction ($\Phi/1$ of PA 200-250 $\Delta t/t_0$ = 50%), as the porosity values do not increase towards the thinnest section of the trailing edge (i.e., ROI 1) cut from the middle of the sample.

Figures 13–16 show CT scans of the analyzed sections of different experimental trailing edges. On the left, three-dimensional reconstructions are displayed. On the right, cross-sections at different heights of the reconstructions are shown. The fine, white line that can partly be seen on the surface of the material in the cross sections marks the surface of the material that has been determined by VG Studio Max 2.1 (VolumeGraphics, Heidelberg, Germany) using the gray values of the measurement. The massive part on the right side of Figure 13b–d is a part of the mounting plate for the set up in the acoustic wind tunnel. It can be seen in all Figures except Figure 14.

A major difference in the pore structure of the displayed experimental trailing edges can be seen, both in the reconstructed volume and the cross sections. The trailing edges made out of PA 200-250 (Figures 14–16) have significantly larger pores compared to the trailing edge out of PA 80-110 (Figure 13). Comparing the trailing edge made out of PA 200-250 as received (Figure 14), to the one out of cold-rolled PA 200-250 with a thickness reduction of 50% (Figure 15) an increased tortuosity can be seen in the latter case, by following one path through each material.

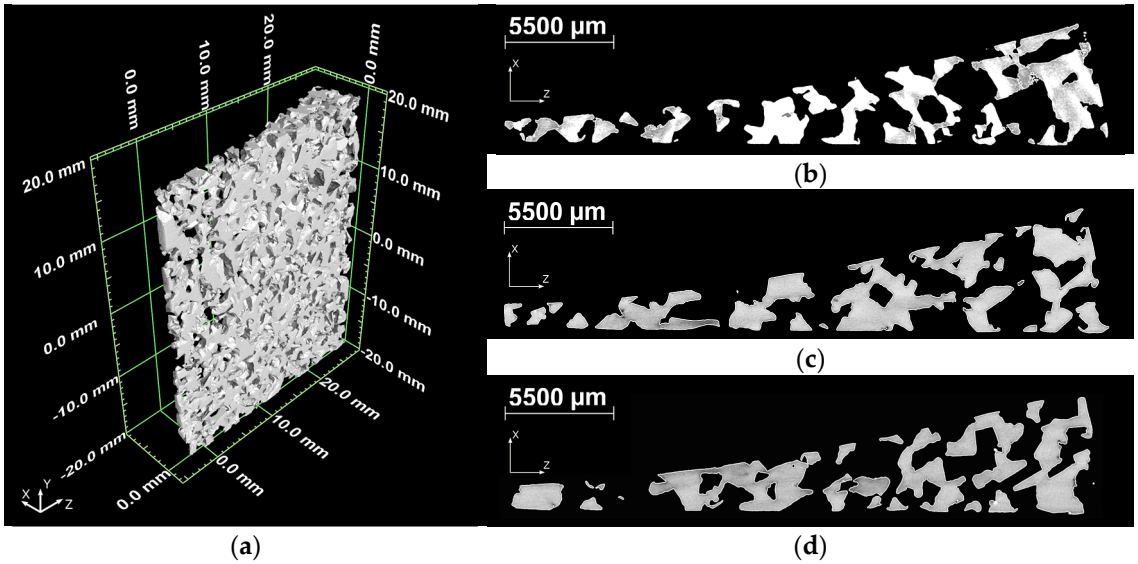

Figure 14. Section of an experimental trailing edge made of PA 200-250 as received. (**a**) reconstructed volume; (**b**) cross section at 10 mm (y-direction); (**c**) cross section at 0 mm (y-direction); (**d**) cross section at −10 mm (y-direction).

Figure 16 shows a trailing edge made out of cold-rolled PA 200-250 with a gradient in thickness reduction from 10 to 50%, as given in Table 2. One can see that the pore structure is changing across the direction of rolling. The pore size and porosity on the right of the cross sections in Figure 16b–d are similar to the overall pore size and porosity of the trailing edge shown in Figure 15 (compare Table 5). The pore size and porosity on the left of the cross sections in Figure 16 is comparable to the pore size and porosity of the material as received (Figure 14). For the trailing edge made out of graded material, the transition from solid matter to the porous material is smooth, with the specific flow resistivity being smallest at the end of the trailing edge. Considering the left of the cross sections, a major part of the pores directly connects the upper and lower side of the material, hence the tortuosity is relatively small. This can be seen in the cross sections of Figure 16b–d as well as in the reconstructed volume (see e.g., green arrows in Figure 16a). Note, that the specific flow resistivity is determined with samples containing several pores in the direction of measurement. If material is thinned to a thickness in the

range of the pore size, the specific flow resistivity changes, as the tortuosity of the material is changed. Thus, the specific flow resistivity of the trailing edges is adjusted by the gradation during cold rolling as well as thinning of the material down to the range of the pore size.

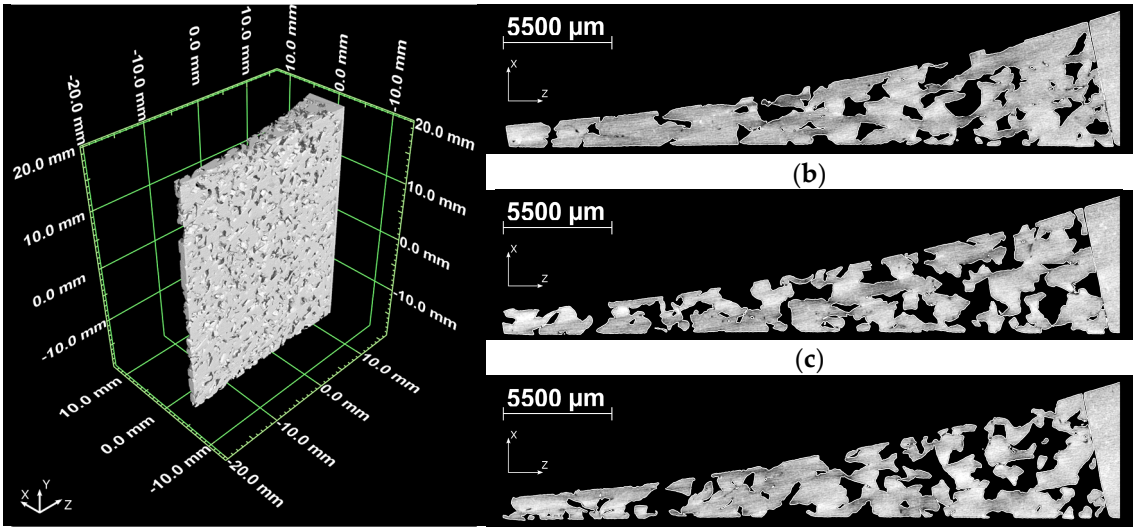

Figure 15. Section of an experimental trailing edge made of cold-rolled PA 200-250 with a thickness reduction of 50%: (**a**) reconstructed volume; (**b**) cross section at 10 mm (y-direction); (**c**) cross section at 0 mm (y-direction); (**d**) cross section at −10 mm (y-direction).

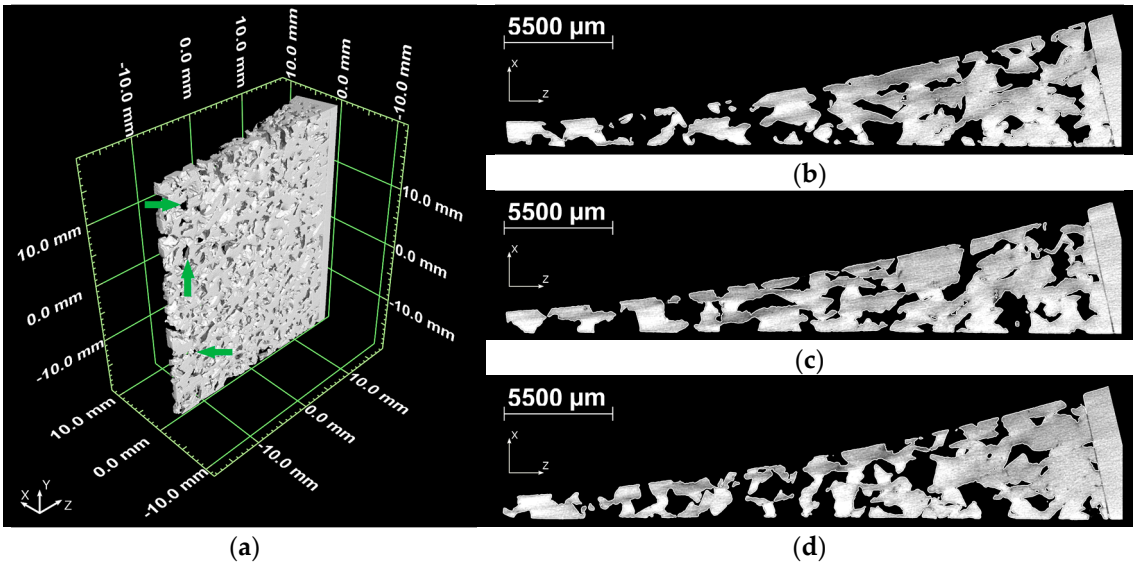

Figure 16. Section of an experimental trailing edge made of cold-rolled PA 200-250 with a gradient in thickness reduction from 10% to 50%: (**a**) reconstructed volume; (**b**) cross section at 10 mm (y-direction); (**c**) cross section at 0 mm (y-direction); (**d**) cross section at −10 mm (y-direction).

4. Conclusions

The results of the experiments show that altering the pore structure of porous aluminum by cold rolling is possible within a wide range of parameters. Using high degrees of deformation even a material with predominantly closed pores can be produced. Thus, a material with a specific flow resistivity from the value of the material as received to very high values can be produced. By using a rolling mill with an adaptive gap between rolls the pore structure was customized during rolling,

leading to a material with a gradient in the specific flow resistivity and porosity. This method allows producing trailing edges with a smooth transition from solid to porous material. This addresses one of the aforementioned shortcomings of porous materials noticed by Herr et al. [6]. Another deficiency of porous materials are the ligaments oriented crosswise to the direction of flow. Lengthening of pores would reduce the number of ligaments for a given length. It was observed during cold rolling in a small range. The acoustic behavior of the material needs to be characterized. Measurements of the material in an acoustic wind tunnel are planned to clarify the influence of the adjusted pore structure. Furthermore, tensile tests show that cold rolling increases the strength of the material, due to a reduction of the pore volume fraction. Comparing the results of the material of the trailing edge used by Herr et al. [6] with the cold-rolled PA 200-250, not only the pore structure was changed as requested, but also the mechanical strength was improved due to cold rolling. Furthermore, discontinuous tensile tests have been performed to show that cold rolling has no negative impact on the damage behavior of the material. Thus, using material with large pores and a small specific flow resistivity (e.g., PA 200-250) as a starting material for cold rolling seems to be a practicable way to specifically alter properties of porous materials (e.g., specific flow resistivity) for the application as a low-noise trailing edge.

Author Contributions: Conceptualization, J.R.; Data curation, J.T. and N.L.; Formal analysis, J.T. and N.L.; Funding acquisition, J.R.; Investigation, J.T., N.L. and J.R.; Project administration, J.T. and N.L.; Supervision, J.R.; Validation, J.T. and N.L.; Visualization, J.T. and N.L.; Writing—original draft, J.T. and J.R.; Writing—review and editing, J.T. and J.R.

Funding: This research was funded by Deutsche Forschungsgemeinschaft (German research foundation) grant number SFB 880 (CRC880).

Conflicts of Interest: The authors declare no conflict of interest. The funders had no role in the design of the study; in the collection, analyses, or interpretation of data; in the writing of the manuscript, and in the decision to publish the results.

References

1. Haines, M.M.; Stansfeld, S.A.; Job, R.F.S.; Berglund, B.; Head, J. Chronic aircraft noise exposure, stress responses, mental health and cognitive performance in school children. *Psychol. Med.* **2001**, *31*, 265–278. [CrossRef] [PubMed]
2. Haines, M.M.; Stansfeld, S.A.; Job, R.F.S.; Berglund, B.; Head, J. Mental Health—A follow-up study of effects of chronic aircraft noise exposure on child stress responses and cognition. *Int. J. Epidemiol.* **2001**, *30*, 839–845. [CrossRef] [PubMed]
3. Franssen, E.A.M.; Van Wiechen, C.M.A.G.; Nagelkerke, N.J.D.; Lebret, E. Aircraft noise around a large international airport and its impact on general health and medication use. *Occup. Environ. Med.* **2004**, *61*, 405–412. [CrossRef] [PubMed]
4. Delfs, J.; Faßmann, B.; Lippitz, N.; Lummer, M.; Mößner, M.; Müller, L.; Rurkowska, K.; Uphoff, S. SFB 880: Aeroacoustic research for low noise take-off and landing. *CEAS Aeronaut. J.* **2014**, *5*, 403–417. [CrossRef]
5. Delfs, J.; Appel, C.; Bernicke, P.; Blech, C.; Blinstrub, J.; Heykena, C.; Kumar, P.; Kutscher, K.; Lippitz, N.; Rossian, L.; et al. Aircraft and technology for low noise short take-off and landing. In Proceedings of the 35th AIAA Applied Aerodynamics Conference, Denver, CO, USA, 5–9 June 2017; American Institute of Aeronautics and Astronautics: Reston, VA, USA, 2017.
6. Herr, M.; Rossignol, K.-S.; Delfs, J.; Lippitz, N.; Mößner, M. Specification of Porous Materials for Low-Noise Trailing-Edge Applications. In Proceedings of the 20th AIAA/CEAS Aeroacoustics Conference, Atlanta, GA, USA, 16–20 June 2014; American Institute of Aeronautics and Astronautics: Reston, VA, USA, 2014.
7. Lippitz, N.; Rösler, J. Analyzing the structure evolution of porous aluminum during cold rolling. In Proceedings of the MetFoam, Barcelona, Spain, 31 August–2 September 2015.
8. Lippitz, N.; Maudarbocus, S.; Rösler, J. The influence of cold rolling on the pore morphology and flow resistivity of porous aluminum. In Proceedings of the Sixth International Conference on Porous Media and Its Applications in Science, Engineering and Industry, Waikoloa, HI, USA, 3–8 July 2016; Engineering Conferences International, Ed.; ECI Digital Archives: New York, NY, USA, 2016.

9. Lippitz, N.; Rösler, J. The influence of cold rolling on the pore structure, flow resistivity and mechanical properties of porous aluminum. In *SFB 880—Fundamentals of High-Lift for Future Commercial Aircraft: Biennial Report*; Radespiel, R., Ed.; TU Braunschweig Campus Forschungsflughafen: Braunschweig, Germany, 2017; pp. 25–33.
10. Lippitz, N.; Rösler, J. Mechanical and structural characterization of porous materials. In *SFB 880—Fundamentals of High-Lift for Future Commercial Aircraft: Biennial Report*; Radespiel, R., Ed.; TU Braunschweig Campus Forschungsflughafen: Braunschweig, Germany, 2015.
11. Hinze, B.; Rösler, J.; Lippitz, N. Noise Reduction Potential of Cellular Metals. *Metals* **2012**, *2*, 195–201. [CrossRef]
12. Hinze, B.; Rösler, J.; Schmitz, F. Production of nanoporous superalloy membranes by load-free coarsening of γ'-precipitates. *Acta Mater.* **2011**, *59*, 3049–3060. [CrossRef]
13. Rösler, J.; Näth, O. Mechanical behaviour of nanoporous superalloy membranes. *Acta Mater.* **2010**, *58*, 1815–1828. [CrossRef]
14. Harders, H. *Fatigue of Aluminium Foam*; Der Andere Verlag: Tönning, Germany, 2005.
15. Ashby, M.F. *Metal Foams. A Design Guide*; Butterworth-Heinemann: Boston, MA, USA, 2000.
16. Lippitz, N.; Rösler, J. Damage Behavior of Sintered Fiber Felts. *Metals* **2015**, *5*, 591–602. [CrossRef]
17. Deutsches Institut für Normung. *Acoustics; Materials for Acoustical Applications; Determination of Airflow Resistance (ISO 9053:1991)*; German Version EN 29053:1993; (DIN EN 29053:1991-05); Beuth Verlag GmbH: Berlin, Germany, 1993.
18. Allard, J.-F.; Atalla, N. *Propagation of Sound in Porous Media. Modelling Sound Absorbing Materials*, 2nd ed.; Wiley: Hoboken, NJ, USA, 2009.
19. Lippitz, N. *Poröse Materialien zur Reduzierung von Hinterkantenschall an Flugzeugflügeln*; Niedersächsiches Forschungszentrum für Luftfahrt: Braunschweig, Germany, 2017.